

ACCURATE SIMULATION OF THE ELECTRON CLOUD IN THE FERMILAB MAIN INJECTOR WITH VORPAL*

Paul L. G. Lebrun, Panagiotis Spentzouris, Fermilab, IL 60510, USA[†]
 John R. Cary, Peter Stoltz, Seth A. Veitser, Tech-X, Boulder, Colorado, USA[‡]

Abstract

We present results from a precision simulation of the electron cloud (EC) in the Fermilab Main Injector using the code VORPAL. This is a fully 3d and self consistent treatment of the EC. Both distributions of electrons in 6D phase-space and E.M. field maps have been generated. This has been done for various configurations of the magnetic fields found around the machine have been studied. Plasma waves associated to the fluctuation density of the cloud have been analyzed. Our results are compared with those obtained with the POSINST code. The response of a Retarding Field Analyzer (RFA) to the EC has been simulated, as well as the more challenging microwave absorption experiment. Definite predictions of their exact response are difficult to obtain, mostly because of the uncertainties in the secondary emission yield and, in the case of the RFA, because of the sensitivity of the electron collection efficiency to unknown stray magnetic fields. Nonetheless, our simulations do provide guidance to the experimental program.

MOTIVATION

The electron cloud (EC) phenomena in high intensity proton storage rings and synchrotrons can limit the performance of such machines [1], [3]. This phenomena is characterized by an exponential growth of the number of low energy (eV) electrons emitted at the surface of the beam pipe wall. Such electrons are then accelerated by the field induced by the passage of the proton beam, which itself causes more secondary emission of electrons at the beam pipe wall. This is reminiscent to the multipacting phenomena observed in R.F. cavities, where one field emission region is replaced the proton beam itself. Such EC can generate fast beam instabilities, as they strongly perturb the electric field in the vicinity of the proton beam. This has been predicted by many models, observed in many e^+e^- storage rings, and studied in detail at CernTA [4]. The Fermilab Main Injector (MI) is no exception. In the “Project X”[5] era, the delivered beam power on target will go from the current value of 300 MW to 2.1 GW. In a first upgrade, the MI cycle time will be reduced to 1.33 seconds from

its current value of 2.2 seconds, thereby increasing the 120 GeV beam power to 700 kW. The second upgrade will require a new injector as the bunch charge will increase by a factor of three. While the MI currently delivers the designed beam intensity, we are concerned that a significant increase of the bunch charge will trigger the formation of a much denser EC, and significantly increase beam losses due to fast instabilities that are hard to control.

Therefore, an R&D initiative has started aiming at providing a robust mitigation strategy. Unlike some e^+e^- storage rings (e.g. KEKB), the MI has relatively short straight sections compared to the length of the arcs, which almost entirely consist of dipoles and quadrupole. Thus, an EC solution based on the use of solenoidal fields that confine the EC away from the beam is simply not applicable. A well established solution would consist in coating the beam pipe with a thin layer of either TiN or amorphous carbon [10], but such a solution could be expensive. Thus, despite the success of numerous previous effort in describing the EC, further R&D on the EC in the MI is well justified, because both the phenomenology and the mitigation strategy have always been site specific.

Furthermore, we present here detailed results on the EC morphology and related fields. This is accomplished using VORPAL [11]. This is a code used for accurate simulation of plasma and beams problems where complicated collective effects are important. Unlike POSINST [3, 7] and QuickPic [6], two distinct codes originally written to simulate “positrons beam instabilities” and used extensively to simulate the response of the beam to the perturbation due to EC, VORPAL is a fully consistent, 3D electromagnetic code using relativistic electrons. Results on a specific benchmark POSINST vs VORPAL will be briefly discussed. While VORPAL allows us to obtain a more precise description of the EC, this can only be done for relatively short sections (2 to 16 m.) of the machine, due to computational limitations. Over such short distances and for relatively short periods of time compared to a full synchrotron cycle, ($\approx 1.0 \mu$ sec), the electromagnetic fields induced by the EC are not strong enough to perturb the trajectories of the ≈ 20 GeV proton beam. Therefore, the proton beam is assumed to be perfectly rigid, i.e., no changes to its associated current occur throughout the simulation.¹

* Work by Fermi Research Alliance, LLC under Contract No. DE-AC02-07CH11359 with the United States Department of Energy.

[†] lebrun@fnal.gov, spentz@fnal.gov

[‡] cary@txcorp.com, pstoltz@txcorp.com, veitser@txcorp.com

¹Evidently, this is not true over long distances and many turns. However, our simulation produces field maps that can and hopefully will be

Finally, new detectors have been developed in the recent past to characterize the EC. In this paper, we report on both the simulation of the EC phenomena and two distinct instruments: the Retarding Field Analyzer (RFA) [8] and the measurement of phase shifts in microwaves propagating in the MI beam pipe [9].

CONFIGURATIONS

The Fermilab Main Injector

The Fermilab Main Injector (MI) is a strong focusing high energy synchrotron. A complete description of it is evidently beyond the scope of this paper, but can be found in our Fermilab operating manuals[12]. The relevant features of the MI are summarized on table 1. Note that one essential parameter, the Secondary Emission Yield (SEY) at the beam pipe wall, is poorly known. While the SEY can be determined on the bench, it is known to be affected by the complicated surface chemistry in presence of residual gas and irradiation due to beam losses, and the electron cloud itself [13, 14].

The pressure is listed for sake of completeness but is not used in this calculation. That is, we limit our study to the exponential-like growth of the EC due to the interaction of the EC with proton beam and the beam pipe walls, skipping over the generation of the seed electrons. It is assumed that some electrons are present in the beam pipe at the beginning of a batch, either due to beam losses or gas ionization. This “seed EC” is much thinner² than the EC due to multipacting between the beam and beam pipe wall. That is, the steady-state EC due to gas ionization is much too thin to cause beam instabilities, by at least 5 order of magnitude, as obviously shown later on. However, other sources for seed electrons, such as those due to beam losses, are harder to determine. This simplification implies that our simulation will not give any ab-initio estimate for the timing of the onset of the disturbing EC.

Regarding the transverse emittance, most of the calculations have been done for the worst case scenario for EC, when the emittance remains small and the transverse fields are the strongest.

Modeling of the relevant section of the machine.

A simulation of the EC throughout the full 3.2 km ring is both unnecessary and unrealistic, as it would require too much compute power. The following setups have been implemented in our simulation:

- Short sections with the large radius beam pipe and with small stray magnetic fields. Such straight sec-

incorporate into the Synergia framework where numerous collective effect can be studied. This will allow us to study the impact of the EC on the beam itself.

²Assuming an ionization production ≈ 28 ions/cm at STP (assuming a typical Hydrogen, water, Nitrogen, CO mixture[15, 16]), per minimum ionizing protons, the seed density due to gas ionization is estimated to be $1.2 \cdot 10^6 e/m^3$

tions contain one meter coated beam pipe that have been instrumented with RFA's.

- Short (0.25 to 1 m. long) sections of a MI dipole, with uniform dipole fields and an elliptical beam pipe.
- Long (~ 16 m.) sections of the elliptical beam pipe with a uniformed magnetic field. The length is determined by the distance between antenna used in the microwave experiment. While such a perfectly uniform magnetic field is not realistic, it has been implemented in the simulation for simplicity and benchmarking purpose.
- Long (~ 16 m.) sections of the elliptical beam pipe with a MI dipole followed by a MI quadrupole, then a dipole. Realistic fringe fields have been implemented.

Throughout this calculation, the MI is assumed to be at ≈ 20 GeV, close to transition, where the bunch length is shortest. This energy has been chosen because the EC effect is most pronounced when the electric fields created the proton bunch are most intense, that is, when the bunches are short. The transverse beam size quoted on table 1 are realistic as they are based on real measurements [18, 19]³. This emittance is in part dictated by the performance of the Fermilab 8 GeV Booster and associated transfer beam lines, the resistive wall instability (mitigated by the use of a damper system [20]), and possibly by the EC effect.

As shown later, the EC is a localized phenomena, particularly in a strong confining magnetic field. Thus, the short sections can be used to study in detail the some dynamical aspect of the cloud with limited compute power. The long section allows us to study the EC for a variety of magnetic fields and are also used for the simulation of the microwave experiment.

The propagation of a bunch train is simulated for about a fraction of one microsecond. Such a short time with respect to the cycle time of the synchrotron or even the duration of one Fermilab Booster batch (1.6μ sec) is justified because the EC quickly reaches saturation (~ 100 ns), if dense enough. If the EC is thin, or evanescent, then longer simulation are needed, but such cases are of little interest, as such ECs will not cause beam instabilities.

Our main simulation tool: VORPAL

VORPAL[11] is a fully 3D code and self-consistent. By this we mean that, within the precision dictated the cell size and the time step, the kinematics of the electrons is correctly dictated by the e.m. field configuration and all fields are taken into account. All such calculations are 3D without requirements on symmetries of the boundary condition. The Courant condition that sets the consistency of the time step regarding to the cell size is always satisfied.

³This is based on recent measurements using the ion profile monitor. Such measurement are a within 10 % of the advertised performance stated in reference [19]

Table 1: Current MI machine and beam parameters.

Parameter	Value
Dipole lengths	6.096 m and 4.064 m
Magnetic Field in dipole (20 GeV)	0.234 Tesla
Number of dipoles	216 and 128
Quadrupole Lengths	2.134, 2.539, and 2.945 m
Quadrupole gradient (20 GeV)	2.25 T/m
Number of quadrupole	128, 32 and 48
Length of all dipoles and quadrupole	2332.7 m
Total Length of MI	3319.4 m
Beam Pipe in the arcs minor/major radii	2.39 / 5.88 cm
Beam Pipe radius in straights	7.46 cm
Beam Pipe Material	16 gauge 316L stainless steel
Secondary Emission Yield 300 eV	1.0 – 3.0
Vacuum	$\approx 2.0 \cdot 10^{-8}$ Torr
Max. Num. of Protons per bunch	$1.0 \cdot 10^{11}$
Longitudinal emittance per bunch	0.8 – 2.6 eVs
Bunch Length	1 m to 0.3 m
Bunch Spacing	18.9 ns
Number of bunch per batch	70
Number of empty bunches between gaps	4
Abort gaps	$2 \times 0.8 \mu\text{sec}$
Maximum number of batch	6
Number of bunches per batch	82
Empty bunches at end of batches	3
Normalized transverse emittance	15 to 25 π mm mRad
$\beta_x \sim \beta_y$ in the arcs	11 to 56 m
Bunch transverse size 20 GeV (r.m.s.)	≈ 3 to ≈ 6 mm
Beam Pipe Frequency Cutoff (in dipoles)	1.49 GHz
Microwave Frequency	1.538 GHz
Space between Emitter/Receiver	~ 13 m

The Furman & Pivi[21] model for secondary emission has been implemented in the Tech-X library [22], which is extensively used by the VORPAL code. In addition, the Vaughan model [25] has been implemented and an arbitrary SEY can be uploaded, allowing us to quantitatively determine the sensitivity of the EC effect to the so-called "true secondary" emission yield.

VORPAL runs on leadership class machine, such as the Blue-Gene P or the Cray. Parallelism is implemented in such a way that the casual user does not need to know nor understand the message passing interface MPI. However, targeted problem decomposition have been used to optimize performance, as discussed below.

EC VORPAL scripts and running conditions. As any general purpose codes, VORPAL needs to be customized to the specific problem at hand. This is done by writing specific scripts, which define the physical configuration of the currents and boundaries, initial condition of the cloud and electron emitters. A summary of the salient parameter is given on table 2

The cell size is dictated by the smallest feature in the problem, which, in our case is either the transverse beam

size, or the physical size of the slits in the RFA's. Systematic uncertainties are estimated by simply looking at relative changes of the relevant quantities, such as the electron density of the EC, or the voltage on the simulated antenna in the case of the microwave absorption experiment, as a function of grid size. Those listed on table 2 are therefore typical and were not rigidly set at the onset of the calculations.

Two distinct types of boundaries are used: The elliptic (or cylindrical) beam pipe, transverse to the beam and the Perfectly Matched Layers (PML). These later types of boundaries simulate an infinitely long beam pipe on either end of the region of interest. They are particularly needed in detecting quasi plasma wave and the simulation of the microwave absorption experiment.

The initial state of the electron cloud is defined as follow. All electrons have negligible velocities, and are distributed uniformly along the beam axis, awaiting the passage of the first bunch. On the transverse plane we have a simple 2D Gaussian distribution, $\approx 3\times$ broader than the beam. Fortunately, the details of this initial state are inconsequential, as they are completely forgotten after the passage of a few bunches. The initial density is set typically

set at $2.5 \cdot 10^{11} m^{-3}$ and the maximum of macro-electrons per cell is initially set to 15. Results at saturation are found to be stable against an increase of such initial conditions.

The static magnetic field configurations (stated above) as well as the current sources are implemented via VORPAL functions and macros. There are two distinct types of current source in the problem: the proton beam itself and the current source responsible for the emission of the microwave generation, only used in the case of the simulation of the microwave absorption experiment.

The electromagnetic solver for cell close to the curved boundary (e.g., the beam pipe) uses the Dey-Mitra [23] cut cell method. A Boris integrator/propagator is used for the relativistic macro-electrons particle. These macro-particles are weighted: as their number grows exponentially at the beginning, the EC is culled and the weights are re-assigned. The probability for a macro-particle to disappear or being re-weighted is flat across the 6D phase space occupied by the EC. At any given time, all weights for all macro-electrons are identical.

The decomposition (i.e., the mapping of PIC cells to computer nodes) is regular and cells that are physically close to each others along the beam axis are preferably implemented on the same processors. This specific decomposition is advantageous because, in most cases, the transverse magnetic field is strong enough to confine the electrons close to the field lines, thereby limiting the transport of electrons along the beam axis. Thus, it make sense to sparsify the problem along the beam axis.

Finally, VORPAL generates multiple output files. Beside the usual log file, the state of the EC is given as a collection of 6D phase space coordinates, the e.m. fields value for each cell and the so-called VORPAL *History* files are extensively used throughout this simulation. These files contain user-specified quantities recorded at every time steps, such the e.m. potential between two points, the number of macro-electrons, allowing us to get a precise detailed picture of selected quantities throughout the simulation.

POSINST

The EC phenomena in the Fermilab MI has been simulated prior to this work [7] using the POSINST. Since VORPAL is a newcomer, it makes sens to compare the results obtained with VORPAL to previous results, and attempt to understand the differences. This benchmark must be at the same time relatively simple and yet relevant to the problem at hand. Thus, a realistic configuration of the beam pipe (elliptical see table 1) and the static magnetic (0.234 T.) is agreed upon. The same grid size transverse and the same SEY parameters are used. To avoid over-simplification, the beam is displaced vertically by 2.5 mm with respect to the center of the beam pipe. A relatively high SEY is used (reaching 2.2 at 300 eV) allowing us to shorten the growth time period and stress the codes, and the final density is higher than for evanescent ECs.

Oral Session

RESULTS

POSINST vs VORPAL: a specific benchmark.

A difference between VORPAL and POSINST relates to the dimensionality: VORPAL can either run as a 2D or 3D code, while POSINST is strictly a 2D+ code. This approximation is fully justified as long as the confining magnetic field is much larger than the transient magnetic field produced by the proton beam: net acceleration of the electrons occurs only along the field lines. Therefore a 2D, time dependent, “electrostatic” calculation is allowed. This has been tested in the VORPAL context, where the 4D proton beam current has been reduced to a time dependent charge density, neglecting the longitudinal current and thereby the magnetic induced by the beam. The VORPAL number of spatial dimension is set to 2. Indeed, the EC density obtained in VORPAL in this 2D and the usual 3D case are consistent.

As shown later, this density changes rapidly near the walls of the beam pipe. Consequently, one has to refine the grid near the curved surface to maintain accuracy. Integrated over the entire volume, changing the transverse grid size from 32×32 to 64×64 changes the estimate of the EC density by 20%. Fortunately, what counts is the EC density in the beam region: the e.m. forces on the protons induced by either free electrons very close to the beam pipe or on the beam surface are small, and nearly identical. Thus, we focused out attention on a 1 beam sigma cylinder centered on the beam. There, the a change of a factor 2^2 in grid size gives at most a 14% change in density.

Since the seed EC are completely different in VORPAL vs POSINST, the onset of the exponential growth can not be compared. Therefore, the POSINST and VORPAL curves have been shifted along the horizontal axes, and only the growth rate (exponential in both codes) and the saturation value can be compared. The details of the EC density at saturation, for POSINST and VORPAL are shown on figure 1. The EC densities in the beam region differ by a factor of ≈ 2 . In addition, the growth rate is slower in POSINST. The root-causes of these discrepancies are currently under investigation.

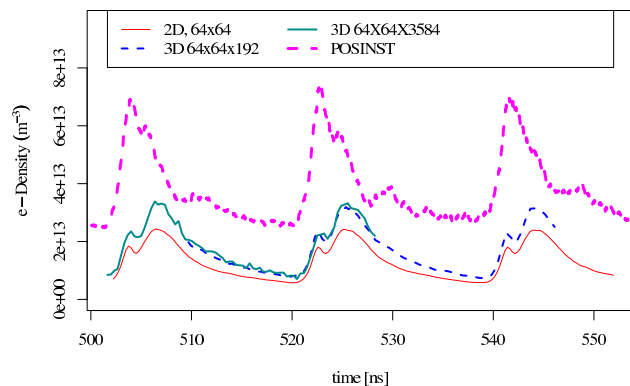


Figure 1: The EC density vs time, once saturation is nearly achieved, for POSINST and VORPAL, in the beam region.

Table 2: Relevant Simulation parameters.

Parameter	Value
Phyla Length	from 0.25 m to 16 m
Beam Pipe geometry	elliptical, or cylindrical, as real
Magnetic fields	See above
Number of Grid cells (small con fig.)	720 X 48 X 24
Number of Grid cells (large con fig.)	6144 X 48 X 48
PM Ls length	≈ 1 to 3 m
Typical Time step	3.12 ps
Typical Num. of time steps	10^5
Typical Num. electrons/cell	20
Typical Nnum of processors	32 to 512
Beam Pipe geometry	elliptical, or cylindrical, as real
Bunch Length	0.3 m
Microwave frequency	1.538 GHz
Microwave Electric Field	20 to 100 V/m
BPM dist. emitter/receiver	3.5 m

Growth rate, saturation and decay rate of the EC.

The EC density, based on a VORPAL calculation, for a few different SEYs is shown on figure 2. The SEY curve follow the Vaughan model[25]. The long section of the beam pipe comprising two dipoles and one quadrupole has been used. A proton bunch intensity of $7 \cdot 10^{10}$ is assumed. Evidently, both the growth rate and the saturation value of the density depends on the assumed SEY. Cases where the initial EC has a very long growth time, or the seed EC diffuses away, have not been studied extensively, as they correspond to an nonexistent EC problem. This occurs for $SEY_{max} \leq 1.3$. Despite the factor ≈ 2 discrepancy in the EC density stated above, this critical SEY_{max} value is consistent with the other 2D codes.

For relatively large $SEY_{max} (\geq 2.)$, the saturation is reached after just a few bunches. Low energy secondary electrons emitted from the wall are no longer accelerated efficiently by the proton beam as they are repulsed by the pre-existing electrons from the cloud. This screening effect is a result of the self-consistency of the PIC simulation. No ad hoc processes have been added to reach, or tune, this saturation. Average over ≈ 1 bunch width, the linear density along the beam axis (i.e., integrated over the transverse dimension) of the EC is about $70 \pm 10\%$ of the linear charge density in the bunch.

In absence of beam, electrons drift back the walls of the beam pipe. The decay rate of the EC is dictated by the average velocity along the magnetic field line. Typical values for this decay time range from 30 to 100 ns. Deviation for a simple exponential are substantial, because this decay is not a stochastic process, but a causal change, where fast electrons disappear first.

Oral Session

Sensitivity of the EC density to the SEY_{max} and the bunch intensity.

A critical issue for the Fermilab High Intensity frontier program[5] is to determine the additional beam disturbances and losses that are putatively caused by an enhanced EC problem. Unfortunately, given the uncertainty in the SEY_{max} for the “scrubbed” (i.e., processed by the beam) MI beam pipe, no reliable *ab-initio* predictions for the EC density and the related electric field maps can be generated at this point in time. However, if a moderate value for SEY is assumed - and this is justified by the fact that the EC problem does not currently limit the performance of the MI -, our result indicates that increasing the bunch intensity will not trigger a significant, non-linear, rise in the EC density, as shown on figure 3. This happens despite an increase of the peak electric field because the SEY no longer increases above ≈ 300 eV.

This happy conclusion seems robust against changes in the beam parameters: More intense bunches is likely to cause an increase the beam emittance (via space charge effects at injection, for instance), which itself implies weaker accelerating fields for the electrons in the cloud. Again, in this regime, the SEY weakly depends on the kinetic energy of the electrons.

Some detailed results on electron kinematics, Electric Field and plasma waves

Prior to discuss the experimental program, various observations on the morphology in 6D phase space of the EC are noteworthy. The spatial (longitudinal and transverse) distribution of the electrons in the cloud are shown on figure 4 and figure 5, respectively. The dynamics is also illustrate there via the rapid (\approx ns) change in the local density of cloud. Except for about one ns just after the passage of the bunch, the highest density is always close to the wall

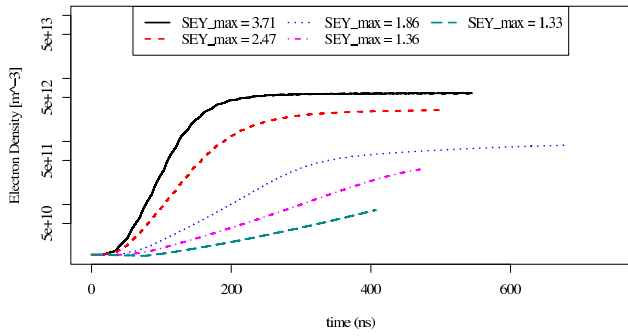


Figure 2: The EC density vs time, at the beginning of a bunch train, for about 10 to 25 MI bunch spacing, illustrating the initial exponential growth and its saturation, if the SEY is high enough. The seed density is arbitrary, but realistic. This illustrates the sensitivity to the maximum of the SEY.

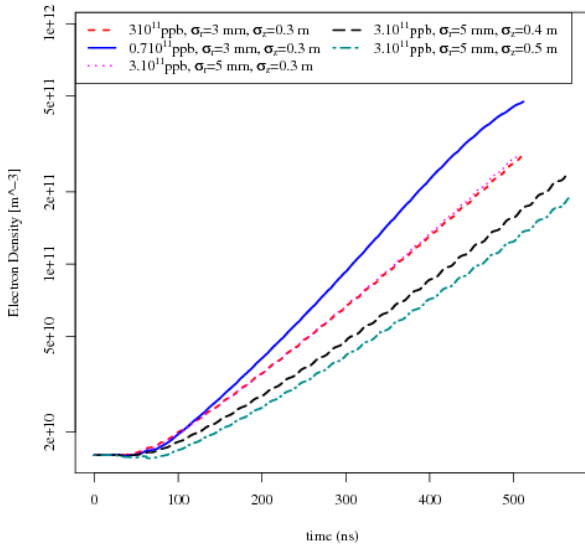


Figure 3: Similarly to the previous plot, The EC density is shown vs time, for various beam conditions. σ_r and σ_z corresponds to the average beam radius and bunch length, respectively. For a moderate value of SEY of 1.36, the worst case scenario corresponds to the current operating conditions and not those expected in the Project-X era.

and can be almost two orders of magnitude higher than at the center of the beam pipe.

The EC density depends on the confining magnetic field, even when the EC is nearly saturated. The fluctuations of the density during and in-between bunches has a non-trivial dependence on this magnetic field, as shown on figure 6 for large SEY_{max} and at stable saturation (i.e., the density averaged over one bunch crossing is stable over time). Also shown on this figure is the mean kinetic energy vs distance from the closest bunch. Highest densities occurs in the drift regions, because net acceleration along the elec-

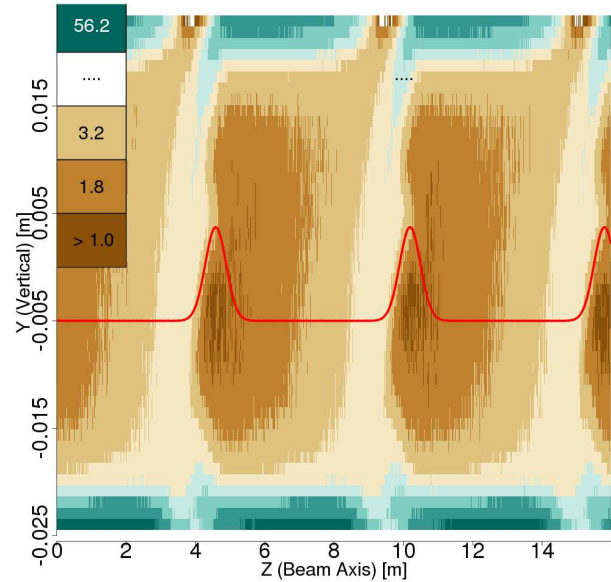


Figure 4: An false color map of the longitudinal profile of the EC density in a dipole and for a continuous bunch train. The color scale is logarithmic. infinitely long dipole and a continuous sequence of bunches. The EC is fully saturated with $SEY_m \approx 2.2$. The proton bunch intensity is $0.7 \cdot 10^{11}$. The proton beam (red line) is displaced by 5 mm downwards, which makes the EC top-down asymmetric.

tric field lines induced by the passage of the proton bunch can occur in all transverse directions. The average kinetic energy is highest in the dipoles, presumably because the electric field created by the bunch, tends to be parallel to the magnetic field lines, allowing for efficient acceleration. Except in the fringe regions, the mean velocity along the beam axis is negligible compared the transverse velocities, even in absence of magnetic field.

For near critical SEY , the EC will vanish in the quadrupoles and be the highest in the field free regions, as shown on figure 7⁴

From these results, it is clear that the EC density fluctuates at 53 MHz (the bunch crossing frequency), with frequency components up to a few GHz (related to the bunch length.) It is also strongly anisotropic, with at least a strong quadrupole component, if not higher multipoles. Thus the EC will produce electromagnetic wave. While the low frequency component can not propagate in the beam pipe (the cutoff for the fundamental mode being at 1.56 GHz), higher order modes are induced and could be detected. In our simulation, the “pseudo-potential”⁵ in between the top and bottom plates of BPMs is recorded for every time step. A straightforward Fourier transform reveals these electromagnetic waves produced by the EC, as shown on figure 8. Evidently, such calculations must be done with the E.M.,

⁴By “field free”, we mean the external $B_x = B_y = B_z = 0$, exactly.

⁵The line integral of the electric field along a specific (and easy to compute) and fixed path, i.e., in our case, along the vertical axis.

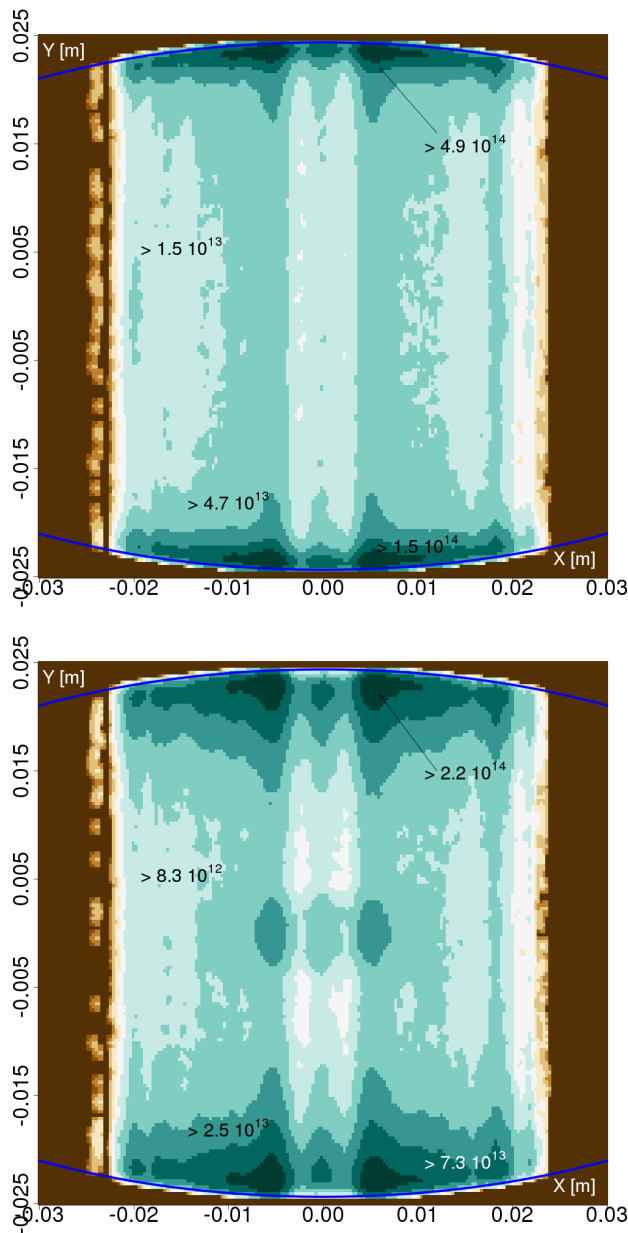


Figure 5: Transverse profile of the EC density. Top: at the beginning of the relaxation phase, when the density reaches a maximum. Bottom: during the pinch phase, when the density is minimum, as the electrons have just migrated away from walls and a diffused excess is seen around the beam spot.

3D VORPAL code and not the relatively 2D code.

As in any complete PIC E.M. code, VORPAL also provided e.m. field maps. Of particular interest is the electric field induced by both the proton beam and the EC, as our ultimate goal is to model these fields such that they can be incorporated in advanced accelerator simulation codes that model non-linear and collective effects [27] Such an example field map is given on figure 9.

Oral Session

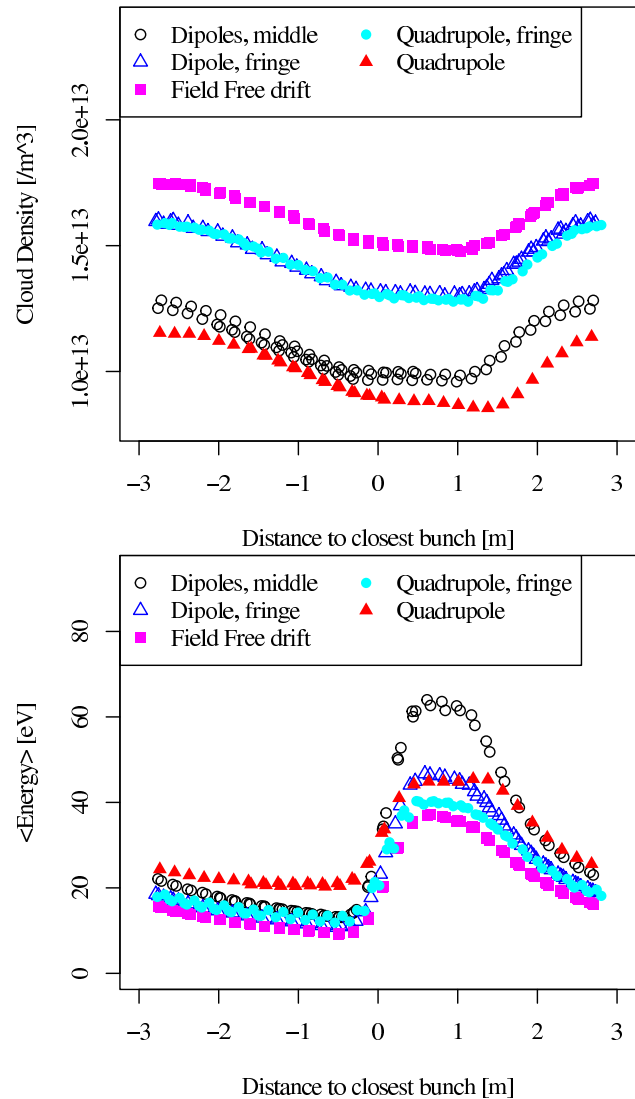


Figure 6: Top: Fluctuation of the EC density averaged over a 40 cm long section of the beam pipe as a function of the distance to the closest proton bunch, for different magnetic field configurations and $0.7 \cdot 10^{11}$ Bottom: based on the same configuration the average kinetic energy of the electrons in the cloud.

On the RFA response

A few Retarding Field Analyzers (RFA) have been recently installed in a field free of the Main Injector, where the beam pipe is cylindrical, 6" diameter [8]. Slits allowing electrons to drift into these devices are located on top or bottom of the pipe and have transverse (longitudinal) openings of about 4 mm (2.5 cm), respectively. In VORPAL, such slits are simulated by simply setting the *SEY* to zero at their location. Fluctuations of the EC density at the slit location can then be extracted from the simulation and are expected to reflect the electron count in these RFAs. An energy cut can be applied to the VORPAL macro-electrons, thereby simulating the effect of the voltage applied on the RFA grid.

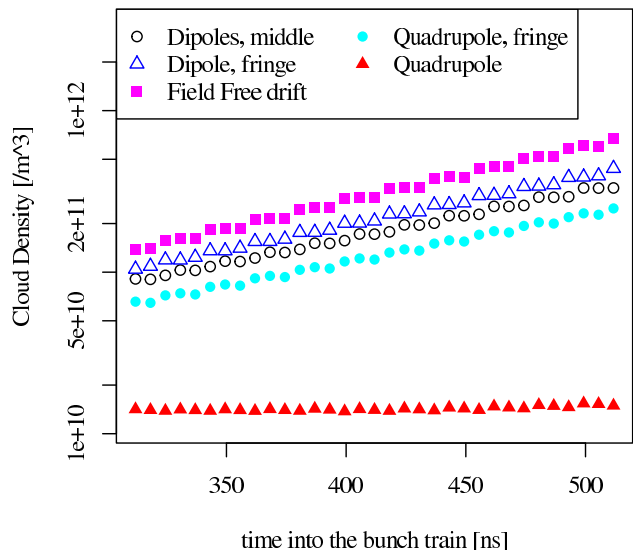


Figure 7: Dependence of the EC exponential growth on the magnetic field configuration, in the case where the *SEY* is near critical.

Abrupt variations of the electric field near the slits (Edge effects) are ignored in this crude simulation. A more exact implementation would include the precise geometry of the RFA grid and its detector. Since these detectors are quite small with respect to the total size of the beam pipe and VORPAL PIC grid has to be uniform, this refinement has not been implemented. However, a much bigger uncertainty comes from the largely unknown stray magnetic fields due to the dipole and quadrupole bus that are running along the beam line. A field of ≈ 3 to 6 Gauss at one of the RFA location has been detected. More detailed maps will be required to compare data to simulation. Meanwhile, as to illustrate the importance of weak magnetic fields in relation to the spatial distribution of the EC, figure 10 shows the transverse distributions of the electrons in the beam pipe for a uniform stray field of 10 Gauss oriented at 45 degrees, perpendicular to the beam axis.

The Microwave absorption experiment

Multiple types of instrument are needed to characterize the EC. Microwave transmission measurements are non-invasive and relatively cheap to implement. The absorption and re-emission of microwave photons by the e-cloud causes a detectable phase shift in this microwave field. This phase shift is related to the density of the e-cloud [28]. Our original intend was to compare our simulation results to real data taken at the MI [9]. However, significant problems were found at a later stage with the measurement technique: The chosen frequency was very close to the cut-off frequency of the elliptical beam pipe (≈ 1.54 GHz) and, consequently, the transmission efficiency was found to be depend critically on the details of beam pipe (pressure valves, bellows, etc) and to actually change during data taking. That is, the effective length between the re-

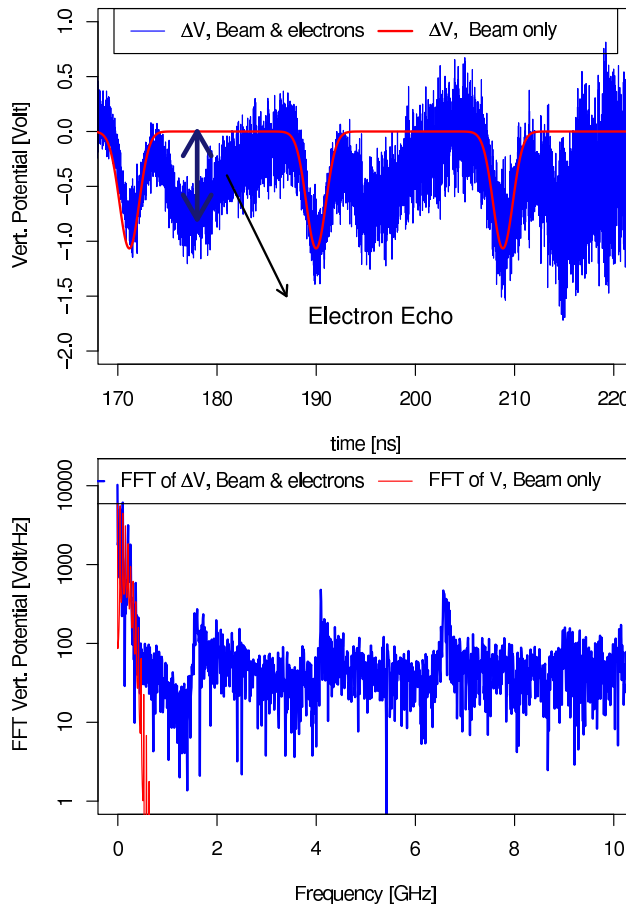


Figure 8: Top: The VORPAL pseudo voltage between the top and bottom plate of a virtual BPM in a dipole, when the beam is displaced vertically by 2.5 mm. In this case where the *SEY* = 2.2 and therefore the EC is saturated. About one ns after the passage of the bunch, the EC re-arrange itself, producing an “echo” signal. Bottom: the Fourier transform of this signal, showing clearly the low frequency cutoff and the higher order mode for this elliptical cavity.

ceiving and emitting antennas was difficult to determine. Yet, for sake of completion, the phase shift calculated for the long (dipole, quadrupole, dipole) section of the MI is shown on figure 11. As in the simple linearized theory, the phase shift is a good measure of the density.

SUMMARY

The electron cloud in the Fermilab Main Injector has been simulated in details using a 3D, self-consistent code, VORPAL. This PIC code is relatively new to our EC community and has been bench marked against the existing POSINST code and current discrepancies are under study. Meanwhile, the self-consistency of our VORPAL results has been checked and details map of the EC density and electric field have been computed. Such field map could be included in the Synergia framework. While the uncertainty in the *SEY* is such that no accurate predictions for the EC

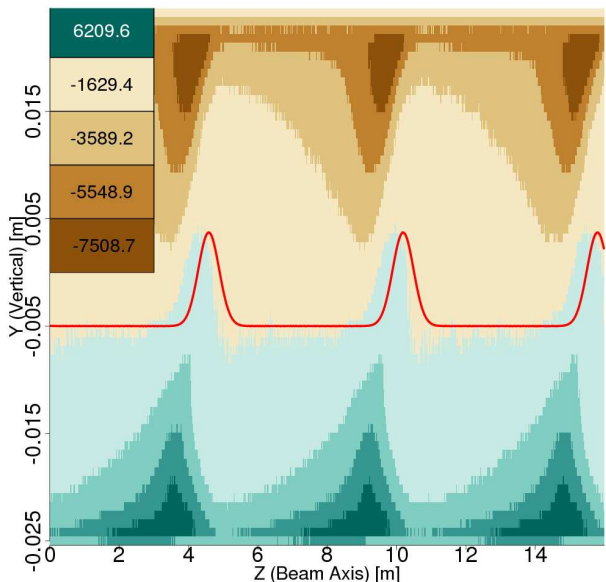


Figure 9: A color map of the projected electric field produced by both the proton bunch and the EC. The setup and beam conditions are those corresponding to the results presented on figure 4.

density can be made in the MI case, our results indicate that if the EC is thin enough not to cause beam instabilities it is then likely that the SEY is rather low (≤ 1.36). In this case, our calculation shows that we should not see a dramatic increase of the EC during the project X era.

Despite the lack of precise predictions for the EC density, this simulation effort is worthwhile, as it provides guidance in establish a robust experimental program. More specifically, the value of the stray magnetic field at the RFA position must be determine. Since the SEY depends on the beam induced scrubbing, this crucial parameter must be determined *in-situ* and inside a magnetic field commensurate with the one used in the dipole or quadrupole. A dedicate set of two small dipoles equipped with instrumentation, retractable sample holder and an electron gun (to measure the SEY) should be installed in one of the available straight section of the MI.

Acknowledgments

We thank Jim Amundson and Bob Zwaska from the Fermilab APC group for very productive discussions on the analysis of the data generated by VORPAL. Xiaolong Zhang ran successfully the POSINST code for the benchmark. We also acknowledge the other members of the VORPAL team: D. Alexander, K. Amyx, T. Austin, G. I. Bell, D. L. Bruhwiler, R. S. Busby, J. Carlsson, E. Cormier-Michel, Y. Choi, B. M. Cowan, D. A. Dimitrov, M. Durant, A. Hakim, B. Jamroz, D. P. Karipides, M. Koch, A. Likhanskii, M. C. Lin, J. Loverich, S. Mahalingam, P. Messmer, P. J. Mullowney, C. Nieter,

Oral Session

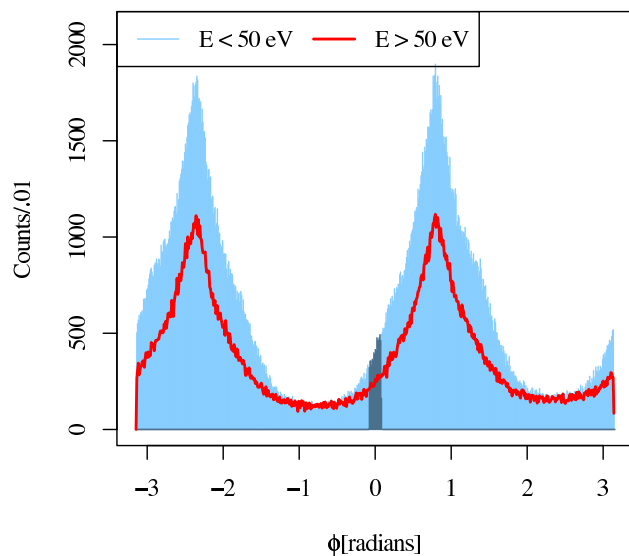
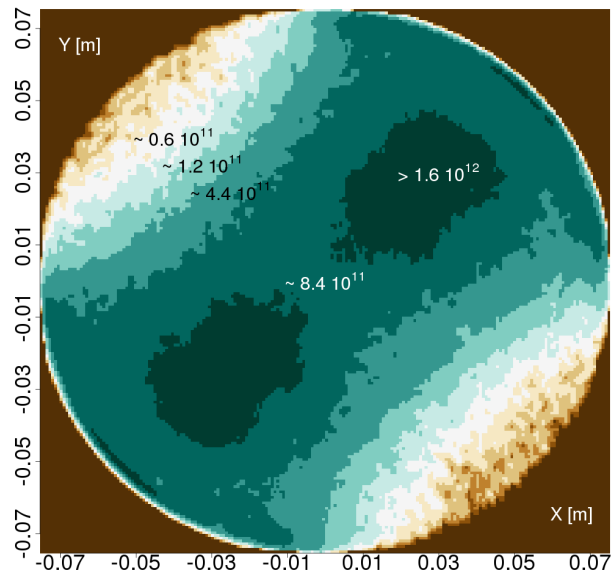


Figure 10: Top: A false color map of the EC density, transverse projection in the circular beam pipe supporting the RFA, as the EC is pinched by the passage of the bunch. The slits of the RFA are highlighted on the top of the cylindrical beam pipe. Bottom: Histograms of the azimuthal angle from the same data set. Again, the highlighted region is where the EC is sampled.

K. Paul, I. Pogorelov, V. Ranjbar, C. Roark, B. T. Schwartz, S. W. Sides, D. N. Smithe, A. Sobol, D. J. Wade-Stein, G. R. Werner, N. Xiang, C. D. Zhou.

This work was supported by the United States Department of Energy under contract DE-AC02-07CH11359 and the CompPASS project funded through the Scientific Discovery through Advanced Computing program in the DOE Office of High Energy Physics. This research used resources of the National Energy Research Scientific Computing Center, which is supported by the Office of Science

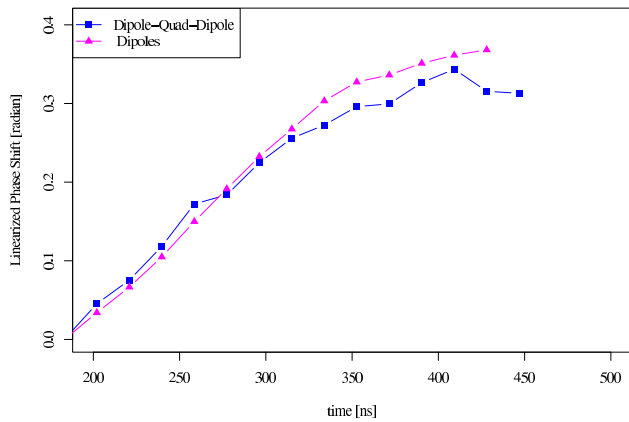


Figure 11: The simulate phase shift for the infinitely long dipole and for a more realistic implementation of a short section of the MI. The setup and beam conditions are those corresponding to the results presented on figure 4.

of the U.S. Department of Energy under Contract No. DE-AC02-05CH11231. This research used resources of the Argonne Leadership Computing Facility at Argonne National Laboratory, which is supported by the Office of Science of the U.S. Department of Energy under contract DE-AC02-06CH11357.

REFERENCES

- [1] Phys. Rev. ST Accel. Beams 7, 124801 (2004)
- [2] A. Z. Ghalam *et al.*, Phys. Plasmas 13, 056710 (2006)
- [3] M. T. Pivi and M. A. Furman, Phys. Rev. ST Accel. Beams 6, 034201 (2003).
- [4] M.A. Palmer *et al.*, “Electron Cloud at Low Emittance in CEsrTA”, IPAC10, Kyoto, Japan, May 2010
- [5] S. Holmes, “Project X: A multi-MW proton source at Fermilab” IPAC10, Kyoto, Japan, May 2010 http://accelconf.web.cern.ch/AccelConf/IPAC10/talks/tuyra01_talk.pdf
- [6] A. Ghalam *et al.*, “3-D parallel simulation of continuous beam-cloud interactions”, in *Proceedings of the 31st ICFA Beam Dynamics Workshop: Electron Cloud Effects*, Napa, CA, 2004, edited by M. Furman, SLAC-PUB-10751 (ECLLOUD04).
- [7] X. Zhang *et al.*, FERMILAB-CONF-07-214-AD (June 2007), Proceedings of Particle Accelerator Conference (PAC07), Albuquerque, New Mexico, 25-29 Jun 2007, pp 3501 <http://accelconf.web.cern.ch/AccelConf/p07/PAPERS/THPAN117.PDF>
- [8] C.Y. Tan, K.L. Duel, R. Zwaska, (Fermilab) . FERMILAB-CONF-09-141-AD, Apr 2009. 3pp. Presented at Particle Accelerator Conference (PAC 09), Vancouver, BC, Canada, 4-8 May 2009.
- [9] N. Eddy *et al.*, FERMILAB-CONF-09-168-AD (May 2009) 3p. Presented at Particle Accelerator Conference (PAC 09), Vancouver, BC, Canada, 4-8 May 2009.
- [10] C. Yim Vallgren, *et al.*, “Low secondary electron yield carbon coatings for electron cloud mitigation in modern particle accelerators”, IPAC10, Kyoto, Japan, May 2010.
- [11] C. Nieter and J. R. Cary, “VORPAL: a versatile plasma simulation code”, J. Comp. Phys. 196, 448-472 (2004).
- [12] The Fermilab Main Injector Technical Design Handbook, http://www.fmi.fnal.gov/fmiinternal/MI_Technical_Design/index.html and The Main Injector Rookie Book, http://www-bdnew.fnal.gov/operations/rookie_books/Main_Injector_v1.1.pdf.
- [13] B. Henrist *et al.*, Proceedings of EPAC 2002, Paris, France, p. 2553 <http://cern.ch/AccelConf/e02/PAPERS/WEPDO014.pdf>
- [14] N. Hilleret *et al.*, Proceedings of EPAC 2000, Vienna, Austria, p. 217 <http://cern.ch/AccelConf/e00/PAPERS/THXF102.pdf>
- [15] J. R. Zagel *et al* Proceedings of the Particle Accelerator Conference, Vancouver, Canada, p. 2166 <http://cern.ch/AccelConf/pac97/papers/pdf/5P052.PDF>
- [16] Sauli, F., Principles of Operation of Multiwire Proportional and Drift Chambers, CERN 77-09, 3/5/1977
- [17] Ed Barsotti *et al* Proceedings of the 1999 Particle Accelerator Conference, New York, 1999 <http://cern.ch/AccelConf/p99/PAPERS/WEA149.PDF>
- [18] I. Kourbanis and D. Capista Private communication, March 2010
- [19] Stephen D. Holmes, Proceedings of the Particle Accelerator Conference, Vancouver, Canada, p. 47 <http://cern.ch/AccelConf/pac97/papers/pdf/2B001.PDF>
- [20] P. Adamson *et al*, Proceedings of the 2005 Particle Accelerator Conference, Knoxville, Tennessee <http://cern.ch/AccelConf/p05/PAPERS/MPPP015.PDF>
- [21] M. A. Furman and M. T. Pivi, Phys. Rev. ST Accel. Beams 5, 124404 (2002).
- [22] . H. Stoltz and M. A. Furman and J.-L. Vay and A. W. Molvik and R. H. Cohen, “Numerical simulation of the generation of secondary electrons in the High Current Experiment”, *Phys. Rev. ST Accel. Beams*, 6, 054701, doi:10.1103/PhysRevSTAB.6.054701, 2003.
- [23] VORPAL reference manual, v4.0, p. 86.
- [24] Wolfgang S. M. Werner *et al* Phys. Rev. **B 78**, 233403 (2008).
- [25] Arnold Shih and Charles Hor, IEEE Transactions on Electron Devices, Vol 40, 4, April 1993.
- [26] M. A. Furman, private communication in the context of the Compass Collaboration, 2008.
- [27] J.F. Amundson *et al* Proceedings of Hadron 2008, Nashville, Tennessee, <http://accelconf.web.cern.ch/AccelConf/HB2008/papers/wga08.pdf>
- [28] Kiran Sonnad *et al*, “Simulation and analysis of microwave transmission through an electron cloud, a comparison and results.” PAC’07, THPAS008, May 2007, Albuquerque, New Mexico, p. 3525, <http://www.JACoW.org>.